A Dynamic Lattice Monte Carlo Model of Ion Transport in Inhomogeneous Dielectric Environments: Method and Implementation

Peter Graf and Abraham Nitzan*

School of Chemistry, Tel Aviv University, Tel Aviv 69978, Israel

Maria G. Kurnikova and Rob D. Coalson

Department of Chemistry, University of Pittsburgh, Pittsburgh, Pennsylvania 15260

Received: April 3, 2000; In Final Form: September 11, 2000

A dynamic lattice Monte Carlo (DLMC) simulation approach to the description of ion transport in dielectric environments is presented. Conventional approaches using periodic boundary conditions are inefficient for nonequilibrium situations in inhomogeneous systems. Instead, the simulated system is embedded in a bigger system that determines the average electrostatic potential and the ionic concentrations at its boundaries. Two issues are of special importance: implementing the given boundary conditions in the treatment of dynamical processes at and near the boundaries, and efficient evaluation of ion−ion interaction in the heterogeneous dielectric medium during the Monte Carlo simulation. The performance of the method is checked by comparing numerical results to exact solutions for simple geometries, and to mean field (Poisson−Nernst−Planck, PNP) theory in a system where the latter should provide a reasonable description. Other examples in which the PNP theory fails in various degrees are shown and discussed. In particular, PNP results deviate considerably from the DLMC dynamics for ion transport through rigid narrow membrane channels with large disparity between the dielectric constants of the protein and the water environments.

1. Introduction

Ion transport in inhomogeneous condensed phases is of considerable interest in many fields of fundamental and applied science. Electrochemical processes dominated by ion transport at interfaces,[1,2] inhomogeneous solid ionic conductors,[3] and ion transport through membrane channels[4,5] are a few prominent examples. The motivation for the present work is the ongoing effort to develop efficient numerical tools for electrochemical processes in confined systems, e.g., ion transport through membrane channels and dynamics of electrolytes near and between dielectric membranes. Full scale molecular dynamics simulations of such systems are still prohibitively expensive, being limited by the long time and lengths scales associated with many processes of interest. Instead, one usually resorts to (a) describing the solvent as a dielectric continuum and (b) describing the ions within the Poisson−Boltzmann (PB) or the Poisson−Nernst−Planck (PNP) mean field approximation. Such approaches (see Appendix A) are widely used for describing ionic equilibrium at and between dielectric interfaces[6] and in inhomogeneous dielectric environments such as proteins,[7,8] and for studying ion transport through biological channels.[9−18] Computationally feasible models of transport in ionic systems that go beyond the continuum level of description have been largely restricted to the treatment of homogeneous systems[19] or to systems of very simple geometries. Recently, Brownian dynamics studies of ion transport through membrane channels have been reported.[20−25] Detailed molecular dynamics (MD) simulations of ionic biological channels are currently limited to short time equilibrium simulations.[26−28] It is expected that such MD simulations will in the future extend and partly replace coarse-grained stochastic approaches to nonequilibrium phenomena. It should be kept in mind, however, that well-reasoned coarse grained descriptions of large complex systems are not merely ways to save computational effort, but routes to focusing on the important aspects of complex systems and processes, where details may be unimportant and nonessential for a consistent description.

The goal of the present work is to develop a possible framework for such a coarse-grained approach to ion transport in inhomogeneous dielectric environments, using a dynamic lattice Monte Carlo (DLMC) model for the description of such processes. In the present approach the underlying solvent molecular structure is replaced by a dielectric continuum and the ions are described as charged particles that move on a dense cubic grid. The treatment of the ion−ion interaction is thus promoted from the continuum mean field level used in the PB and PNP levels of description, and the model can describe ion−ion correlations that are disregarded by mean field theories. Similar DLMC models were previously used in studies of ion equilibrium dynamics in glassy and polymer electrolytes;[29−31] however, these studies were limited to infinite macroscopically homogeneous systems without dielectric boundaries.

It should be emphasized that the use of a continuum dielectric picture for the solvent and the boundaries in the present model constitutes a gross simplification, sometimes oversimplification, by disregarding the molecular structure of the solvent. Moreover, the response of the continuum dielectric environment to the ion motion is usually taken linear, local, and instantaneous. Still, simulations that describe ions as individual particles constitute a substantial advance over continuum mean field theories that describe ions as continuous charge distributions. Such approaches, e.g., PB and PNP approximations, are considered useful in many applications, and the present approach can be used to gauge their limits of validity. In particular, we expect that the proposed DLMC approach will be useful when the process studied is driven, or is strongly affected, by correlations between individual ions. In this respect our method is equivalent to the recently advanced Brownian dynamic scheme.[20−24,25a] The

10.1021/jp001282s CCC: $19.00
Published on Web 12/01/2000

latter has the advantage that it is an off-lattice procedure and that it can (in principle) describe short time inertial effects. For the applications of interest to us here (and those described in refs 20−24 and 25a) the latter issue is not very important. The lattice-based approach is numerically less demanding, in particular in the on-lattice mode used here where the same lattice is used for the ion positions and for the grid on which the electrostatic problem is solved. It is important to note that the methods developed here to handle potential and concentration boundary conditions can be adapted also to the off-lattice Langevin approach, as well as to any particle simulation that uses these boundary conditions.

At the core of the numerical approach described below is the embedding of a relatively small system, in which "detailed" numerical simulations (here at the DLMC level) are done, in a larger system whose size prohibits such detailed calculations. In the latter, outer system, theory, experimental information, or computation on a more coarse grained level is used. In principle, one would like to develop a numerical procedure in which coarse grained (e.g., continuum level) computations in the outer system and detailed (e.g., particle) simulation on the inner system are brought together into a consistent union.[32,33] The calculation described below accomplishes this goal in the following way: We assume that theory or coarse-grained calculation done on the outer system can provide boundary conditions for the motions of particles in the inner system and examine the dynamics of the latter under these boundary conditions. The cycle would become complete when data from the inner system, properly coarse grained, are fed back as input to the calculation done on the outer system. Even at the present incomplete stage one can get useful information on ion transport in inhomogeneous dielectric systems, as shown below.

This paper is organized as follows: In section 2 we briefly review the electrostatic background needed in later sections. In section 3 we sketch the general layout of systems that we want to investigate, in order to set the stage for the remaining sections. Sections 4−7 elaborate on critical issues pertaining to the computation of interaction energies and the DLMC simulation and outline our approach to these issues. A simple application is demonstrated in section 8 and concluding remarks follow in section 9. Explicit formulas and technical details are given in the Appendices.

2. Outline of the Problem

We are interested in ionic motion in dielectric media. Dynamics in the system is driven by electrostatic interactions derived from the Poisson equation:

$$-\nabla\cdot[\epsilon(\mathbf{r})\nabla\phi(\mathbf{r})] = 4\pi\rho_{\text{free}}(\mathbf{r}) \qquad (1)$$

where ρ_{free} is the density of free charges, ϕ is the electrostatic potential, and ϵ is the dielectric response. The latter is assumed local in space and time on our coarse-grained scale. In our applications we consider systems composed of different regions characterized by their dielectric constants. This implies that $\epsilon(\mathbf{r})$ is a discontinuous function, a fact that should be carefully addressed in numerical solutions of eq 1.

The Poisson eq 1 has to be supplemented by appropriate boundary conditions. It is important to make a conceptual distinction between two types of boundary conditions that we term "intrinsic" and "imposed". Intrinsic boundary conditions arise from the real physical boundaries of the system. For example, a metal electrode is, in a coarse-grained electrostatic picture, an intrinsic boundary characterized by a given constant potential. In contrast, imposed boundary conditions are artificially introduced into a computational model in order to render the system into a manageable size. Periodic boundary conditions, usually imposed in simulations of infinite homogeneous systems or of systems with local inhomogeneities and short-range interactions, exemplify this type.

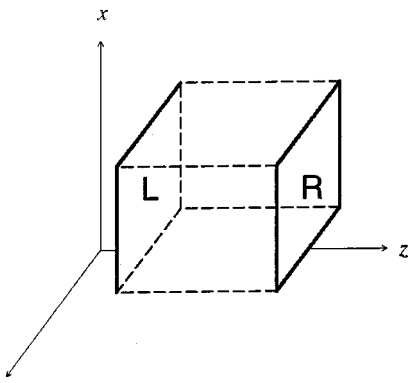

Figure 1. Computational cell: A parallelepiped with concentration and potential boundaries on the planes R and L perpendicular to the *z*-axis. Periodic boundary conditions are taken in the *x*- and *y*-directions. See section 2 for discussion.

Periodic boundary conditions cannot be used to model processes that are (a) relatively local and (b) driven by intrinsic boundaries that are far from the significant local region. For example, ion transport through a biological membrane channel is driven by intrinsic potential and concentration boundary conditions which are set far ($\sim$1 μm) from the channel openings. At the same time the process is controlled by the channel properties. A full scale simulation that connects both the channel and the intrinsic boundaries is not feasible. Instead, one imposes boundary conditions at convenient locations near the channel openings.[9−16] Concentrations and potentials can be imposed at these artificial boundaries using input from theory or from a more coarse grained computation, e.g., a calculation that uses mean field approximations. Problems associated with setting and handling such imposed boundary conditions are central issues in the present work.

To see in more detail the kind of problems that may be encountered in setting up such imposed boundaries, consider a homogeneous electrolyte solution that may be in equilibrium or in a current carrying steady state. We wish to consider in microscopic detail ionic motion in a limited subspace denoted by the parallelepiped in Figure 1, using potential and concentration boundary conditions obtained from theory or from a mean field calculation done in the bigger system. As stated above, periodic boundary conditions are not convenient for simulations of systems that carry fluxes. Potential boundary conditions in homogeneous systems may be replaced by a constant uniform electric field applied to the ions, but this cannot be done in nonhomogeneous systems. Similarly, concentration gradients have to be considered explicitly.[34] As we shall see below, naive application of such imposed boundary conditions can lead to erroneous unphysical results.

As an example consider the plane R in Figure 1, separating two parts of the physical system. To its left we describe the ions as microscopic particles and to its right we are given the average electrostatic potential and ionic concentrations. A naive application of this input is to use the values of these average potential and concentrations as boundary conditions on the plane R in a simulation that follows the motion of individual ions on its left. However, if we attempt to move these ions with a constant electrostatic potential imposed on R, this plane will

behave as a metal surface that attracts ions by image interactions—a gross distortion of the correct dynamics. This artifact will be somewhat compensated by another artifact associated with a naive imposition of concentration boundary conditions: ions in the bulk of an electrolyte solution are solvated by counterions. When they approach a surface with a given fixed salt concentration they lose up to half of this contribution to their solvation energy. They are therefore effectively repelled by such a boundary.

These artifacts arise because, by replacing the given average potential and concentrations by strictly constant values of these variables on a boundary, we disregard important correlations between an ion approaching the boundary and the instantaneous electrostatic potential and ionic concentrations on the boundary. These considerations will guide us below in designing ways to avoid such artifacts or to compensate for them.

Assuming that we can correctly handle these boundary issues, eq 1 yields a solution of the electrostatic problem for a given ionic configuration in our system. The evolution of this configuration is carried out by a dynamic Monte Carlo procedure that uses an energy criterion to evolve the system. This is done by comparing energies corresponding to different configurations of the mobile ions (see section 4). These energies are computed from the work W required to assemble each of these configurations in the presence of the dielectric

$$W = \frac{1}{8\pi}\int \mathbf{D}(\mathbf{r})\cdot\mathbf{E}(\mathbf{r})\, d^3r = \frac{1}{2}\int \rho_{\text{free}}(\mathbf{r})\phi(\mathbf{r})\, d^3r \qquad (2)$$

where $\mathbf{D}$, $\mathbf{E}$, ρ_{free}, and ϕ are respectively the displacement and electric field, the density of free charge and the electrostatic potential. Note that W is a thermodynamic quantity, the change in the Helmholtz free energy of the system due to the introduction of the mobile charges.[21]

The use of eq 2 implies the need to repeatedly solve the electrostatic problem (1). Specifically, we will require the potential $\phi_{j\leftarrow k}$ at position $\mathbf{r}_j$ given an ion at $\mathbf{r}_k$. This is the Green's function, i.e., the solution of eq 1 for $\rho_{\text{free}}(\mathbf{r}) = \delta(\mathbf{r} - \mathbf{r}_k)$ for the given boundary conditions.[36,37] This Green's function contains the effect of the dielectric and the boundary condition. We note in passing that the symmetry property

$$\phi_{j\leftarrow k} \equiv \phi_{k\leftarrow j} \qquad (3)$$

holds regardless of the geometrical structure of the dielectric medium.[35−37] Equation 3 can be derived from the mathematical formulation of the problem,[36] but it can also be justified from a physical consideration: the work of assembly is independent of the particular order in which free charges are introduced into the system.[35,37] The symmetry property (3) will be useful below (sections 6c.3 and Appendix C) for reducing the numerical effort associated with evaluation of the ion−ion interactions.

3. System Geometry and Layout

The inner systems considered in this article have the general shape of a parallelepiped contained in an outer system (Figures 1 and 2). On the left and right boundaries of the computational box, denoted L and R, constant average electric potentials (ϕ_L,ϕ_R) and salt concentrations (c_L,c_R) are prescribed. The other boundaries are treated by periodic boundary conditions.[24] In some applications we will consider a dielectric slab separating the inner system into two regions (Figure 2a). The dielectric constant ϵ_s in the slab differs in general from the dielectric constant ϵ_B of the other two ("bathing") regions. With a narrow pore passing through the slab, this is a primitive model for an ion channel in a biological membrane (Figure 2b).

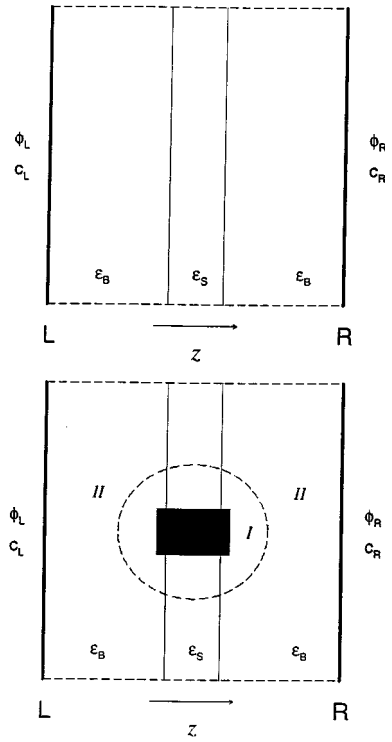

Figure 2. A cross section of the parallelepiped of Figure 1 with particular internal structures: (a, top) a membrane, (b, bottom) a membrane with a pore. See section 3 for discussion. Regions I and II in Figure 2b are used for computational purposes (see Appendix C).

The numerical procedure described in the following sections is not limited to any shape or dielectric properties of the membrane or the pore; however, simple geometries can be exploited to reduce numerical effort. For example, in the simulation of ion transport through a pore in a dielectric membrane (Figure 2b and section 8), the boundaries L and R are set to be at some distance from the fixed charges and dielectric interfaces that define the underlying system. (Mobile ions can be located anywhere in the system.) Under these conditions we divide the interior system into two regions, I and II (Figure 2b). Region I in Figure 2 comprises the pore and some part of the bathing regions and is in general significantly smaller than the remaining part II. The fact that the dynamics is controlled by processes which take place in region I may now be exploited in order to reduce numerical effort by treating interactions involving particles in region II approximately (see Appendix C). We emphasize that the boundary conditions imposed on the L and R boundaries do not represent intrinsic properties in the spirit discussed in section 2, and that the input for ϕ_L, ϕ_R, c_L, and c_R originates from information on the average magnitudes of these variables.

For computational purposes, the system is mapped onto a discrete lattice (Appendix B). In our current implementation the same discrete lattice is used for the numerical solution of the Poisson equation and for defining the configuration space for mobile ions. In particular, each ion occupies one grid cell and can move to adjacent grid cells. Thus, the grid cell defines the ion size and excluded volume interaction is applied by not allowing more than one ion on a grid cell. These restrictions could be eased to allow, e.g., treatment of different ion sizes.[39]

After mapping the general geometry onto the discrete lattice, each of the boundaries L and R may be regarded a dielectric layer with thickness equal to the grid spacing h, that adjoins a

similar layer in the interior of the system. Ions can be exchanged between the boundary layers and the adjacent interior layers in a way that takes into account the given concentration boundary conditions.

The following sections detail issues pertaining to the dynamic Monte Carlo simulation (section 4), the different contributions to the electrostatic energy (section 5), numerical computation of electrostatic interactions (section 6), and the treatment of concentration boundaries (section 7).

4. Dynamic Monte Carlo Simulation

In the dynamic lattice Monte Carlo procedure,[40] particles are placed on grid points in the system and a sequence of configurations is generated by random changes in the positions of the particles and acceptance of a new configuration by an energy criterion. The total simulation length, expressed as a number of cycles, is assumed to be proportional to the real time. (In a cycle the number of individual MC steps is equal to the number of particles in the system.)

We have chosen a transition probability for a single step which is commonly used in the treatment of the kinetic Ising model.[41] Given a current configuration 1 and a random trial configuration 2, the criterion whether the next configuration will be 2 or 1 depends on the energy difference ΔW between the configurations. A uniform random deviate $0 \le r < 1$ is generated. If

$$r < \frac{1}{1 + \exp[\beta \Delta W]} \tag{4}$$

the next configuration is taken to be 2. Otherwise, the current configuration 1 is carried over. In eq 4, $\beta^{-1} = k_B T$, where k_B is the Boltzmann constant and T is absolute temperature.

The fluctuating number of particles poses a certain problem in dynamic Monte Carlo methods because a cycle, which defines the time scale, is constructed relative to the number of particles in the system. We deal with this problem by considering our system as part of a bigger system with a fixed number of particles given by $\tilde{N} = N + N_L + N_R + N_v$. N is the number of particles in the inner system (a fluctuating integer), N_L and N_R are the (fixed) numbers of particles on the left and right boundaries, obtained by integrating the given boundary concentrations c_L and c_R over the volumes of the boundary layers (defined in section 3). These numbers are in general nonintegers. The number $N_v > 0$ of external or virtual particles fluctuates so that $\tilde{N} =$ constant, and is chosen large enough so that the total number $\tilde{N}$ can accommodate, with high probability, the largest fluctuation in N. This is done for counting purposes only: A cycle is defined to consist of $\tilde{N}$ steps. In each step, a particle from the whole system is chosen randomly; however, a new step is attempted, i.e., a new trial configuration is generated, only if the chosen particle is not a virtual particle. This normalization defines our clock time in accord with the actual number of particles in the system. Based on a random walk of noninteracting particles on a cubic lattice, and on the form (4) for the transition criterion, the total simulation time T_S is then related to the number of Monte Carlo cycles N_C by

$$T_S = \frac{h^2 N_C}{12D} \tag{5}$$

where h is the grid spacing and D is the diffusion coefficient of a single ion moving in the dielectric environment. The latter is taken the same for all mobile ions and is assumed known. $D = 10^{-5}$ cm^2/s was used in all the calculations presented in this work.

5. Energetics

This section provides a general description of the energy terms that contribute to ΔW of eq 4. A detailed description of these terms and their computation is given in sections 6 and 7.

The required ΔW is the difference between the electrostatic free energies W of two consecutive configurations. In principle, the electrostatic free energy in a system of ions, dielectric interfaces, and potential boundary conditions can be obtained by computing the energy required to charge the ions in the presence of the given interfaces and boundaries. Such a procedure cannot be used here in a straightforward way because it would yield an energy that contains the unphysical image contributions discussed in section 2. Instead we need a procedure for calculating the electrostatic energy that will yield only the physical contributions to the charging energy. We have found that different procedures are needed to achieve this goal for different contributions to the electrostatic free energy. We therefore represent W as a sum of several distinct contributions

$$W = W^{stat} + W^{self} + W^{coal} + W^{diel} + W^{corr} \tag{6}$$

The possibility to write eq 6 as a superposition of various contributions is of course due to the linearity of the dielectric system. The first term (the sums below are over all ions in the inner system)

$$W^{stat} = \sum_j q_j \phi_j^{stat} \tag{7}$$

is the energy of individual ions in the local electrostatic field arising from static charges and from the source of the imposed (Dirichlet) boundary condition; see section 6a. As discussed in section 6d, this term is further corrected by subtracting the effect of image charge on the imposed boundary to the internal inhomogeneous charge distribution when such a distribution exists.

Next, the term

$$W^{self} = \sum_j \frac{q_j^2}{2} \phi_j^{self} \tag{8}$$

is the self-energy (or solvation energy) of individual ions in the inhomogeneous dielectric environment, computed as described in section 6b.

Turning to the interionic Coulomb interaction, it is convenient to separate it into two terms. The first

$$W^{coul} = \frac{1}{2} \sum_{i \neq j} \frac{q_i q_j}{\epsilon_B} \phi^{coul}(r_{ij}) \tag{9}$$

is the energy associated with the direct Coulombic interaction between pair of ions in a reference homogeneous dielectric environment with dielectric constant ϵ_B. An explicit expression for ϕ^{coul} in our bounded grid is given by eq 14 below. A second term

$$W^{diel} = \frac{1}{2} \sum_{i \neq j} q_i q_j \phi_{i \leftarrow j}^{diel} \tag{10}$$

is the energy resulting from pair of ions interacting via polarization charges induced at internal dielectric interfaces. It

is computed as described in section 6c. Finally

$$W^{\mathrm{corr}} = \sum_j \langle \Phi_j^{\mathrm{corr}} \rangle \tag{11}$$

is a correction to the solvation energy that accounts for the effects of ions outside the inner systems, see section 7.

A slight modification to the configurational energy difference $\Delta W = W_2 - W_1$ is needed for transitions $1 \rightarrow 2$ that involve the system's boundary. If for example the ion of charge q moves from the inner system to the left boundary then W_1 is given by eq 6 computed for N (say) ions, while W_2 is obtained from (6) computed for $N-1$ ions and supplemented by $q\phi_{\mathrm{L}} + q^2/(2\epsilon_{\mathrm{L}}a)$, where ϵ_{L} is the dielectric constant in the left continuum. (The inclusion of the solvation term $q^2/(2\epsilon_{\mathrm{L}}a)$ is done in order to be consistent with the way the energy is computed in the interior side.)

The following two sections deal with the technical details associated with setting and using the boundary conditions imposed on the simulated (inner) system. Section 6 deals with implication of the electrostatic boundaries and section 7 focuses on effects of the concentration boundaries. These analyses yield the energy terms summarized above. A reader who wishes to skip these technical details can proceed to section 8.

6. Computation of Electrostatic Interactions

This section details the use of eq 1 and the associated boundary conditions to obtain the configurational energy of a given distribution of ions in our system. It is convenient to consider separately four contributions to this energy: (1) The interaction with the local field that results from the external field imposed on the system and from the fixed charge distribution present in the system. This contribution is represented by W^{stat} in eq 6. (2) The electrostatic self-energy of an individual ion, W^{self} in (6). (3) The electrostatic ion−ion interactions give rise to the terms W^{coul} and W^{diel} in eq 6. (4) For inhomogeneous charge distributions there is an image response to the average charge distribution. The corresponding energy is included in the term W^{stat}. All these contributions to the configurational energy are affected by the existence and geometry of the internal dielectric interfaces and by the imposed boundaries of the simulated system. An additional energy term, W^{corr} in eq 6, that arises from the contribution to the ion's solvation energy from ions outside the inner system is discussed in section 7.

(a) Single-Particle Electrostatic Energy. Given the electrostatic boundary condition and the distribution of fixed charges, the electrostatic potential in the interior inhomogeneous dielectric system is obtained from the Poisson equation

$$\sum_j L_{ij}\phi_j^{\mathrm{stat}} = \rho_i^{\mathrm{fixed}} + \rho_i^{(\mathrm{D})} \tag{12}$$

where the matrix L is defined in Appendix B, ρ^{fixed} is the distribution of fixed charges on the grid, and $\rho^{(\mathrm{D})}$ is the "source" term associated with the imposed (Dirichlet) boundary conditions on the R and L surfaces. The corresponding contribution to the electrostatic energy of an ion of charge q_j at grid point j is $q_j\phi_j^{\mathrm{stat}}$.

(b) Dielectric Self-energy. In a uniform dielectric, the self-energy of an ion is essentially its Born solvation energy. In an infinite uniform system this self-energy is position independent and does not affect the ionic distribution and dynamics. This is no longer true in a heterogeneous dielectric, where the position dependence of the ion solvation energy translates into forces that affect ionic motion and equilibrium distribution. In principle, this contribution to the potential and force experienced by the ion can be computed by modeling the ion as a sphere of radius a with charge q distributed uniformly on its surface, and by solving the Poisson equation with this ion as source given the system boundaries and dielectric structure. Taking an ion of charge q centered at position $\mathbf{r}_k$ as the sole single source, this procedure yields the electrostatic potential $\phi_{s\leftarrow k} = \alpha(\mathbf{r}_k)q$ on the ion surface, where α depends on the system boundaries and dielectric structure but not on the charge q. The self-energy is then

$$\frac{1}{2}q\phi_{s\leftarrow k} = \frac{1}{2}\alpha(\mathbf{r}_k)q^2 \tag{13}$$

This way for numerical evaluation of the self-energy in a finite computational box poses two problems: (1) An *imposed* Dirichlet boundary (e.g., the L and R boundaries of Figures 1 and 2), on which a fixed potential is prescribed, behaves as a metal boundary and attracts individual ions by image interactions. As already discussed, this attractive interaction is not physical: the potential on the imposed boundary is constant only on the average, and its instantaneous value changes when an ion from the interior system approaches it. The correct self-energy of any individual ion should therefore not include this image interaction. The procedure that leads to eq 13 does include this artifact, and a way to remove it should be employed. (2) The result obtained from a grid-based procedure may depend on the grid. This has no consequence for a uniform dielectric where the difference between grid and continuum results is position independent; however, we should consider potential artifacts that may arise in grid representations of nonuniform systems.

We have found that both these problems can be resolved by correcting the potential in eq 13 using the following procedure:

1. Define the truncated bare Coulombic potential of a singly charged ion

$$\phi^{\mathrm{coul}}(r) = \begin{Bmatrix} \frac{1}{a} - \frac{1}{r_{\mathrm{c}}} & r < a \\ \frac{1}{r} - \frac{1}{r_{\mathrm{c}}} & a < r < r_{\mathrm{c}} \\ 0 & r_{\mathrm{c}} < r \end{Bmatrix} \tag{14}$$

where r is the distance from ion center, a is the ion radius,[42] and r_{c} is an imposed cutoff distance.[43] Outside the parallelepiped of Figures 1 and 2, the potential (14) is mapped according to the minimum image condition in the x- and y-direction perpendicular to the current. In our implementations, all ionic radii are set to $a = h/2$ and r_{c} is taken equal to $L_{xy}/2$, where h is the grid spacing and L_{xy} is the linear size of the L and R boundaries taken as squares.

2. A discretized Laplacian matrix $L^{(0)}$ is constructed for our finite lattice ($L^{(0)}$ corresponds to the $\epsilon \rightarrow 1$ limit of the more general matrix L defined in appendix B).

3. A lattice charge distribution is constructed by operating with the lattice Laplacian on the potential (14):

$$\rho_{i\leftarrow k}^{\mathrm{coul}} = \sum_j L_{ij}^{(0)}\,\phi_{i\leftarrow k}^{\mathrm{coul}} \tag{15}$$

In eq 15, i and j are points on the 3-dimensional discrete grid and $\phi_{j\leftarrow k}^{\mathrm{coul}}$ is the potential (14) computed on grid point j for an ion located at position k. The corresponding operation in continuous space would give the original charge distribution.[44] On the finite grid, however, where the discretized Laplacian

$L^{(0)}$ reflects the discretization and the boundary conditions,[45] this correspondence is no longer exact. Instead the resulting charge distribution on the grid corresponds to the grid representation of the potential (14).[46]

4. The actual potential, $\phi_{j\leftarrow k}$, associated with the lattice charge distribution (15) that corresponds to an ion placed at point k, is obtained from solving the full Poisson equation including all dielectric boundaries, using the charge distribution (15) as an input

$$\sum_j L_{ij}\phi_{j\leftarrow k} = \rho^{\text{coul}}_{i\leftarrow k} \tag{16}$$

where the full Poisson matrix L is defined in Appendix B.

5. The self-energy of the ion is given by

$$\phi^{\text{self}}_k = \frac{1}{2}\phi_{k\leftarrow k} \tag{17}$$

If the point $\vec{r}_k$ is not on the grid, $\phi_{k\leftarrow k}$, may be obtained by interpolation. The result (17) is for a singly charged ion. The self-energy of an ion of charge q placed at point k is $q^2\phi^{\text{self}}_k$.

The method described by eqs 14−17 is clearly heuristic. In essence, it describes the charged particle not by the given charge distribution but by a lattice charge distribution $\rho^{\text{coul}}_{i\leftarrow k}$ that would yield the cutoff Coulomb potential (14) for $\epsilon = 1$, in the presence of the imposed potential boundary conditions. The resulting self-energy contains contributions from all internal dielectric interfaces, but not the unphysical image interaction associated with the imposed boundary.[47]

As a test of this procedure, we compute the dielectric self-energy experienced by an ion of size $a = h/2$ in a system containing a single dielectric interface

$$\epsilon = \begin{Bmatrix} 80 & z < 0 \\ 2 & z > 0 \end{Bmatrix} \tag{18}$$

The real space lattice size was chosen $L_x \times L_y \times L_z = 128 \times 128 \times 66$ Å. The system is finite in the z-direction with zero electrostatic potential (with the meaning and implications discussed above) imposed on the L and R surfaces perpendicular to the z-direction and positioned at $z = \pm 33$ Å. Periodic boundary conditions (with the minimum image convention used for the ion charge) are used in the x- and y-direction. The lattice spacing, which corresponds to the distance of closest approach of two ions and to the step size for the movement of mobile ions, was taken $h = 2$ Å. The same parameters are used for all other applications presented in this work.

Figure 3 shows the dielectric self-energy of a singly charged ion ($q = e$, where e is the magnitude of the elementary charge) as function of its position along the z-axis in comparison with the corresponding analytical result[48] obtained for an infinite system. The result verifies the validity of the numerical procedure proposed above.

A similar procedure could be used also to evaluate the ion−ion interactions on the grid, however we have opted to evaluate the latter by a different method that is described next.

(c) Ion−Ion Interactions. Next consider the contribution to the overall energy from ion−ion interactions. For ions of unit charge in infinite space with uniform dielectric constant ϵ it is $(\epsilon r)^{-1}$ where r is the interionic distance. In the presence of dielectric inhomogeneities, it can be conveniently thought to be a sum of two parts: (1) a $1/r$ Coulomb interaction, essentially $(\epsilon_B r)^{-1}$, screened by the dielectric constant ϵ_B of a uniform reference bath and (2) contributions from dielectric polarization charges that result from dielectric inhomogeneities measured relative to the uniform bath. For singly charged ions a distance r apart, the first part is $\phi^{\text{coul}}/\epsilon_B$, where ϕ^{coul} is given by eq 14, and should be multiplied by the actual ionic charges q_iq_j. Another contribution, the interaction of one ion with the image on the external potential boundary of another ion, is unphysical as discussed above, and should be excluded. The following procedure calculates the second part while excluding the unphysical image contribution:

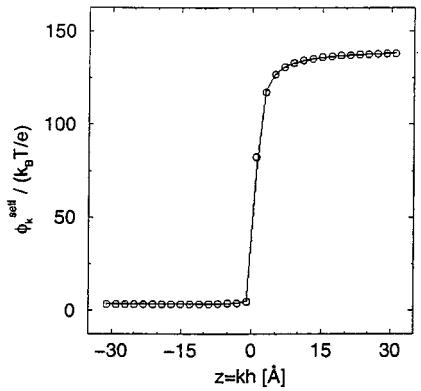

Figure 3. Dielectric self-energy of a singly charged ion as a function of its position z in a system characterized by the inhomogeneous dielectric constant eq 18. The computational system is finite in the z-direction; see text for details. Circles, numerical results; full line, analytical result in an infinite system. $T = 298$ K is used in the normalization of the potential value, and e is the electron charge.

1. An ion of unit charge positioned on a lattice point is represented by a charge density $\rho_{i\leftarrow k} = \delta_{ik}/V_h$ where V_h is the volume of a lattice cell.

2. The grid Poisson equation is solved twice: once for an ion location on a grid point k in a uniform bath with dielectric constant ϵ_B

$$\sum_j L^B_{ij}\,\phi^B_{j\leftarrow k} = \frac{\delta_{ik}}{V_h} \tag{19}$$

(see Appendix B for the definition of L^B), and once for the same ion in the actual inhomogeneous dielectric

$$\sum_j L_{ij}\phi_{j\leftarrow k} = \frac{\delta_{ik}}{V_h} \tag{20}$$

3. The relative dielectric contribution to the electrostatic interaction between singly charged ions at j and k is obtained from the difference

$$\phi_{j\leftarrow k} = \phi_{j\leftarrow k} - \phi^B_{j\leftarrow k} \tag{21}$$

This difference eliminates the bare ionic interaction that was obtained separately and leaves the interaction associated with the induced polarization charges. Note that the imposed potential boundary conditions are used in both eqs 19 and 20, so the resulting potentials include the unphysical image contributions of the type discussed in section 6b. These contributions are, however, canceled in the difference (21).[49] The overall interaction energy between two ions at $\mathbf{r}_j$ and $\mathbf{r}_k$ is given as the sum of the two contributions evaluated above:

$$\phi^{\text{int}}_{j\leftarrow k} = \frac{1}{\epsilon_B}\phi^{\text{coul}}_{j\leftarrow k} + \phi^{\text{diel}}_{j\leftarrow k} \tag{22}$$

This result is for singly charged ions and should be multiplied

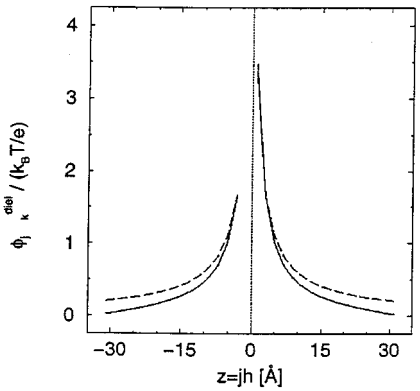

Figure 4. Dielectric contribution to the potential of an ion in the inhomogeneous dielectric system defined by eq 18. The dotted line marks the interface between the two dielectric media and the source is located 1 Å to the left of this line. $\epsilon_B = 80$ is used in the calculation. Full line, numerical result based on eq 21; dashed line, analytical result for an infinite system. All parameters are as in Figure 3.

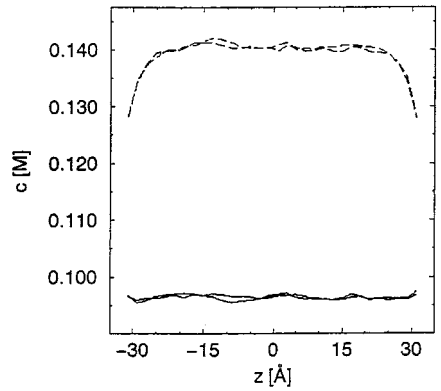

Figure 5. Salt concentration profile in an equilibrium system simulated with (full line) and without (dashed line) the solvation correction discussed in section 7. The salt concentration on the boundaries is set to $c = 0.1$M. The standard parameters given in section 7 are used.

by the ionic charges q_jq_k of the actual ions in these positions. Note that the proposed method preserves the important symmetry property eq 3. In particular, the symmetry

$$\phi^{\mathrm{diel}}_{j\leftarrow k} \equiv \phi^{\mathrm{diel}}_{k\leftarrow j} \tag{23}$$

is due to the fact that the Poisson equation is discretized such that the matrix L is symmetric (see Appendix B). Equation 23 can be utilized to save computational effort in the dynamic Monte Carlo simulation, as discussed in Appendix C.

A test of this procedure is shown in Figure 4. The system is the same as that used in Figure 3. Now the ion is in a fixed position k, one site away from the dielectric interface on the high ϵ-side. The same high value of ϵ, $\epsilon_B = 80$, is taken for the reference environment.[50] The potential $\phi^{\mathrm{diel}}_{j\leftarrow k}$ is plotted as function of the position j along the z-direction. In comparison, the analytical result[48] for an infinite half-space with the same dielectric boundary is shown. The observed small difference results from the image response on the imposed boundaries to the polarization of the internal dielectric interface and will become smaller when the distance between the imposed boundaries and the internal dielectric interface increases. In our calculations we disregard this small error.

(d) Image Response to the Average Charge Distribution. We have argued above that even though we assign a given potential on an imposed boundary, this boundary condition should not affect image response to an individual ion approaching such a boundary. If, however, the average steady-state charge distribution in the interior system is not uniformly zero, the Coulombic potential of this charge distribution should induce image response on the imposed boundary so as to keep the potential on this boundary (i.e., the average potential in the real system) at its prescribed value. In contrast to the image of an individual ion at its instantaneous position, this image corresponds to a real physical interaction that has to be taken into account. This is done using the following procedure:

1. A MC simulation is carried for a certain stretch of steps and the Coulomb potential $\phi(b) = \sum_k \phi^{\mathrm{coul}}_{b\leftarrow k}/\epsilon_B$ on the boundary is accumulated and averaged over this stretch ($\phi^{\mathrm{coul}}_{b\leftarrow k}$ is the value of the truncated bare Coulomb potential, eq 14, induced by an ion at point k, on the boundary point b). The result of this calculation is the potential induced by the averaged charge distribution on the imposed boundaries in a background solvent of dielectric constant ϵ_B. The effects of this potential should actually be canceled by the image response to the averaged charge distribution.

2. The Laplace equation with the matrix $L^{(0)}$ is solved using the potential boundary condition $\phi(b)$ obtained in this way. This yields a potential in the interior system that should be canceled by the image response to the average charge distribution.

3. The dynamic MC procedure is carried for another stretch of MC steps where now the negative of the potential obtained in step 2 is added to the interior potential. This correction to the interior potential accounts for the image charge induced on the boundary by the interior charge distribution. This stretch of the run yields a new $\phi(b)$ that may be different from that obtained from the previous stretch.

4. This procedure is repeated until convergence, which is achieved when the boundary potential $\phi(b)$ and the associated correction to the inner potential do not change appreciably between consecutive stretches.

The effect of this correction is demonstrated below (see Figures 6 and 7 and the related discussion).

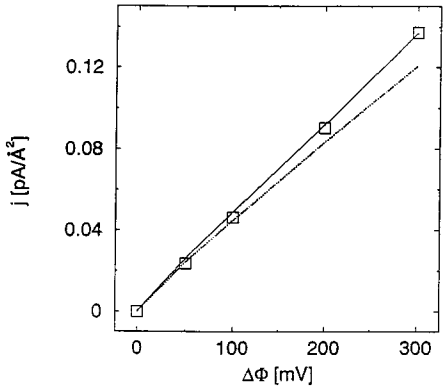

Figure 6. Current vs voltage in the liquid junction described in section 8, characterized by the boundary conditions $c_L = 0.1$ M and $c_R = 0.01$ M. Full line, PNP results; squares, DLMC results. Dotted line, result obtained without the correction due to the image of the average charge distribution.

7. Boundary Effects on Ion Solvation Energies

This section considers another effect associated with the artificial nature of the imposed boundaries—the unphysical loss of ion solvation energy when it approaches a concentration boundary. For simplicity of the presentation we consider a homogeneous equilibrium system.

Consider the parallelepiped in Figure 1, an enclosure in an otherwise infinite equilibrium system, inside which we wish to

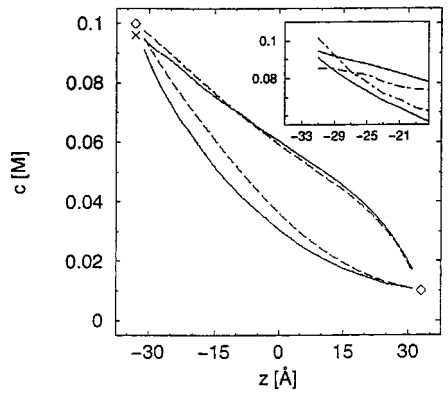

Figure 7. Concentration profiles for the positive (upper lines) and negative (lower lines) ions in the system of Figure 6 for an applied voltage $\Delta\Phi = \phi_L - \phi_R = 100$ mV. Full lines, DLMC results; dashed lines, PNP results. The diamonds on the upper left and lower right of the figure are the imposed concentration boundary conditions at $z = \pm 32$ Å. The cross on the upper left corresponds to the $c_L = 0.096$ M, the bulk concentration obtained in the DLMC calculation at equilibrium with $c_L = c_R = 0.1$ M (see Figure 5). In the inset the concentration profile near the left boundary is shown: full lines are the same DLMC results shown in the main figure. Dashed-dotted lines, results obtained without the correction due to the image of the average charge distribution.

follow the motions of individual ions. Accordingly, we set the equilibrium concentrations and potential (the latter can be taken to be zero) as boundary conditions on the L and R surfaces of the parallelepiped. The neglect of correlations between an ion in the interior system and the boundary leads to the ion seeing different environments close to the boundary and away from it. Physically, a complete ionic atmosphere cannot form around an ion close to the boundary, and the computed energy of such an ion will reflect this lack of solvation. In particular, ions on the boundary layer itself are not automatically subjected to inter-ion interactions that lead to this contribution to their energies. Since our Monte Carlo procedure relies on the configurational energy of the instantaneous ion distribution, such errors in energy will be reflected in the resulting equilibrium distribution and nonequilibrium dynamics. This shortcoming of the computational model may be remedied by adding a suitable average potential, a solvation correction, to the sites near and at the boundary.[51]

To determine this solvation correction we first carry an equilibrium simulation without this correction (called "pass 0") and determine the potential of mean force $\langle\Phi_j^{pmf}\rangle$ at grid point j experienced by an individual ion. The potential of mean force determines the concentration profile in equilibrium systems.[52] By symmetry, the potential of mean force is the same for positive and negative ions of the same absolute charges, so the average over both types can be taken. In addition, the conditional mean potential, $\langle\Phi_j^{cmp}\rangle$, due to ion−ion interactions in the interior of the system near the boundary is determined as the average product of the electrostatic potential exerted by all other ions at the position of a given ion times the charge of that ion.

Both $\langle\Phi_j^{pmf}\rangle$ and $\langle\Phi_j^{cmp}\rangle$ are measured relative to their values in the interior solution far from the imposed boundaries. Their dependence on the position j reflects the artificial nature of the imposed concentration boundaries and should be compensated for. The solvation correction $\langle\Phi_j^{corr}\rangle$ to the single ion energy when moving from an initial to a final site in the inner system or on the boundary is then defined by

$$\begin{aligned}\langle\Phi_j^{corr}\rangle &= 0, \quad \text{in the layer adjacent to the boundary, when the boundary is a source, i.e. when moving from the boundary into that layer}\\ &= -\langle\Phi_j^{cmp}\rangle, \quad \text{in the layer adjacent to the boundary, when the boundary is a sink, i.e., when moving from that layer into the boundary}\\ &= -\langle\Phi_j^{pmf}\rangle, \quad \text{for a site of the interior system when moving to/from another site of the interior system}\end{aligned} \tag{24}$$

Next, a new simulation ("pass 1") is carried out in the presence of these solvation corrections. Note that the correction to the energy difference ΔW in eq 4 is the difference between two such correction terms computed for the corresponding sites. The result yields corrections to $\langle\Phi^{cmp}\rangle$ and $\langle\Phi^{pmf}\rangle$. This procedure is iterated and convergence is achieved when the solvation correction determined from successive simulations varies less than, say, 1% of the thermal energy. For our range of systems, a series of three to four passes was required to determine a sufficiently converged solvation correction.

The effect of this correction is shown in Figure 5, which depicts the equilibrium concentration profile obtained from carrying the dynamic lattice Monte Carlo procedure on an interior system with a univalent binary salt for which the concentration boundary conditions were set to be $c_L = c_R = 0.1$ M. The same parameters, $T = 298$ K, $\epsilon_B = 80$, $h = 2$ Å, $L_x \times L_y \times L_z = 128 \times 128 \times 66$ Å as in Figures 3 and 4 were used. The full lines in the figure show the concentration profiles for the positive and negative ions obtained when the boundary solvation correction is applied. The dashed lines show the concentration profiles obtained without imposing the correction on the simulated system. Note that the exact concentration profiles for the positive and negative ions are identical in this system.

An exact procedure should give uniform equilibrium concentration profiles, $c = 0.1$ M, for both ion types. The uncorrected procedure gives interior ion densities considerably higher than the imposed boundary concentration because of the larger solvation stabilization in the interior. This problem is eliminated in the simulation that includes the solvation correction. In fact we note that the density in the corrected system is about ∼5% lower than the prescribed density on the boundaries. In principle, we could eliminate this overshoot in the correction procedure by slightly adjusting the correction energies in eq 24; however, in the calculations reported below this small error was disregarded.

In practical applications of the solvation correction some further approximations are used. First, the correction is obtained in the way described above for a series of homogeneous equilibrium systems with different salt concentrations, then applied also for nonequilibrium systems. Second, the solvation correction is applied at each boundary L and R, irrespective of the presence and the location of the other boundary. Finally, at a certain distance from the boundaries, the correction gets smaller than, say, 1% of the thermal energy k_BT and is simply ignored. Clearly, these approximations are better for higher temperature and for larger system sizes in the z-direction.

Note that there is a slight asymmetry in the treatment of the energy differences between configurations when a move into or out of the boundary is involved. The asymmetry is a result of the artificial nature of the imposed boundary conditions and appears explicitly in the definition (24) of the solvation correction. In this sense, the configurational energy (6) depends

on the next configuration in the Monte Carlo sequence. This is consistent with the appearance in eq 4 of only energy differences ΔW between two consecutive configurations.

8. Numerical Examples

In this section we present numerical results obtained using the procedure described above for three different systems: a simple liquid junction, a uniform dielectric membrane, and a membrane with a narrow cylindrical pore.

Consider first the simple liquid electrolyte junction. This is a homogeneous electrolyte system characterized by given potentials and salt concentrations on opposite parallel boundaries. The solvent is a homogeneous dielectric with a dielectric constant ϵ_B, so the system has no internal dielectric discontinuities. This system has been extensively explored on the mean field level.[53−55] It is indeed expected that mean field, i.e., Poisson−Boltzmann (PB) and Poisson−Nernst−Planck (PNP) theories, should provide reasonable descriptions of equilibrium and of steady-state conduction in this case. We can therefore use the comparison between the dynamic lattice Monte Carlo (DLMC) procedure developed here and these mean field results in order to assess the working of our particle simulation procedure.[56]

In the simulation presented below the system consists of a monovalent salt of equal size ions dispersed in a continuum dielectric solvent of dielectric constant $\epsilon_B = 80$ contained in a parallelepiped (Figure 1) whose dimensions are $L_x \times L_y \times L_z = 128 \times 128 \times 66$ Å. Periodic boundary conditions are applied in the *x*- and *y*-directions while in the *z*-direction potential and concentration boundary conditions are applied: we assume charge neutrality on these boundaries and take $c_L = 0.1$ M and $c_R = 0.01$ M for the salt concentrations on the left and right boundaries, respectively. The voltage $\Delta\Phi = \phi_L - \phi_R$ is varied from zero up to several tenths of a volt. As before, the grid spacing that corresponds also to the ion size is taken 2 Å. The diffusion constant for all ion types was taken $D = 10^{-5}$ cm^2/s.

Figures 6 and 7 compare the results obtained from the DLMC simulations and PNP calculation on this system. Figure 6 shows the current−voltage characteristic of this junction. Good agreement is seen between the two calculations. Figure 7 shows the average concentration profiles of the positive and negative ions obtained for the same boundary concentrations and for $\Delta\Phi =$ 100 mV. Good agreement between the PNP and the DLMC results is seen on the right, low concentration side, but deviations between the two sets of results appear toward the higher concentration left side. Some of this deviation is due to the remaining ∼5% error in the response of the bulk salt concentration to the imposed boundary condition in equilibrium (see Figure 5 and the related discussion). The ionic concentrations near the left boundary tends toward the salt concentration 0.096 M (marked with a cross in Figure 7), which is the equilibrium interior concentration obtained when a boundary concentration 0.1 M is imposed (see Figure 5), rather than toward the real boundary concentration 0.1 M (marked with a diamond in Figure 7).

Also shown in Figure 6 and the inset to Figure 7 is the effect of neglecting the correction discussed in section 6d—the effect of the image, on the imposed boundary, to the average charge distribution in the inner system. It is seen that neglecting this effect leads to an unphysical behavior of the ion concentration profiles near the boundary, and to a substantial deviation in the current−voltage characteristic in Figure 6.

Next consider the system represented by Figure 2a: a parallelepiped containing an electrolyte in a solvent of dielectric

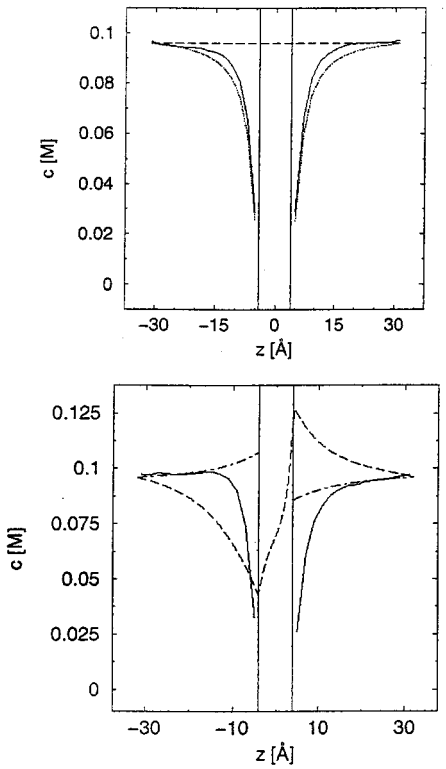

Figure 8. Concentration profiles for the system depicted in Figure 2a, with $\epsilon_B = 80$, $\epsilon_S = 2$, $L_z = 66$ Å, and $l = 8$ Å. $c_L = c_R = 0.1$ M was used in the DLMC calculations while $c_L = c_R = 0.096$ M was used for the PB and PNP calculation. (a) $\Delta\Phi = 0$. Full line, result of the DLMC calculation; dashed line, PB calculation (the corresponding calculation with reflecting membrane−electrolyte interfaces gives zero concentration inside the membrane); dotted line, result from a PB calculation supplemented by the single ion dielectric self-energy. (b) $\Delta\Phi = 100$ mV. Full line, DLMC results; dashed and dashed−dotted lines are PNP results without and with reflecting boundary condition on the membrane−electrolyte interfaces, respectively.

constant ϵ_B, now divided by a dielectric layer, a membrane, of dielectric constant ϵ_S, with $\epsilon_S < \epsilon_B$. The dielectric profile of this system satisfies

$$\epsilon(z) = \begin{cases} \epsilon_B & l/2 < |z| < L_z/2 \\ \epsilon_S & |z| < l/2 \end{cases} \tag{25}$$

where l is the membrane thickness. In the calculation described below we used $\epsilon_B = 80$ and $l = 8$ Å, and boundary concentrations $c_L = c_R = 0.1$ M[57] The applied voltage $\Delta\Phi = \phi_L = \phi_R$ is varied between zero and several tenth of a volt. The electrolyte is a monovalent salt and the lattice is constructed as in the previous example. Figure 8a shows the results obtained for this model for $\epsilon_S = 2$ and $\Delta\Phi = 0$. This is an equilibrium situation that in the mean field level is often analyzed using the Poisson−Boltzmann (PB) theory. Figure 8a depicts the salt concentration profile obtained from the PB theory (dashed line) and from the DLMC calculation (full line). Note that the PB approximation predicts a uniform salt concentration even across the membrane. This approximation involves only the local charge density that remains zero everywhere, while the salt density is constant. This is an artifact resulting from the absence, in this approximation, of short-range repulsion between ions. In reality, the membrane constitutes a high dielectric barrier that repels ions because of the loss in self-energy (Born solvation energy) in the low ϵ-region. It is important to note that this repulsion extends into the high dielectric constant region. A common approximation that supplements the PB procedure by

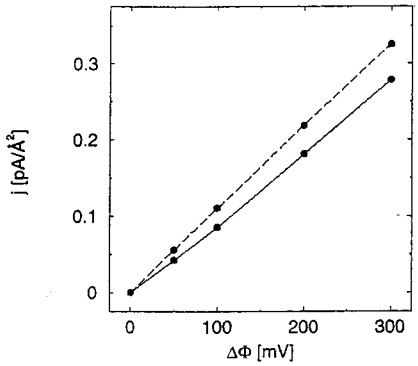

Figure 9. Current vs voltage characteristic of a system similar to that of Figure 8, except that $\epsilon_S = 60$. Full line, DLMC results. Dashed line, PNP result.

imposing zero flux (reflecting) boundary conditions at the membrane boundaries ($z = \pm l/2$) yields a salt distribution that is represented outside the membrane by the dashed line in Figure 8a and is zero inside the membrane. If, instead, we compute the ion self-energy as described in section 5.2 (this is a single-particle property that can be computed and stored at the start of the calculation) and use it to supplement the ion's energy in the PB calculation, we obtain the result represented by the dotted line of Figure 8a.

Similar results for the nonequilibrium steady-state characterized by $\Delta\Phi = 100$ mV are shown in Figure 8b. Here the DLMC result (full line) is compared to the results obtained from the mean field PNP calculation without (dashed line) and with (dashed−dotted line) reflecting boundary conditions at the membrane surfaces. This lines represent the concentration, $c_+(z)$, of the positive ions. Because of the symmetry of the problem, the negative ion concentration is given by the mirror reflection about the center of these lines.

For the examples shown in Figure 8, the dielectric barrier computed from the single ion self-energy is found to be $\sim 110 k_B T$ ($T = 300$ K). (For a thick membrane this barrier can be estimated from the difference between the Born self-energies, $(q^2/(2a))(1/\epsilon_s - 1/\epsilon_B)$. With our parameters it yields $\sim 137 k_B T$). This barrier is too high to yield any appreciable current in the situation described by Figure 8b. Indeed no barrier crossings were observed in the DLMC simulation during simulation ($\sim 10^6$ Monte Carlo cycles), which therefore essentially describes two disjoint equilibrium subsystems. In contrast, the PNP calculation yields under these conditions a net current of 10^3 A/cm^2. In this respect the imposition of reflecting boundary conditions at the membrane-electrolyte interfaces, blocking current in and across the membrane, reflects the correct physics. This cannot be done, however, when the dielectric barrier is lower so appreciable current can flow. Figure 9 shows current vs voltage curves obtained for such a situation. Here $\epsilon_B = 80$ as before while ϵ_S was taken 60, yielding a dielectric barrier of about $1 k_B T$ for $T = 300$ *K*. The deviation of the PNP result (dashed line) from the DLMC result (full line) is again related to the fact that PNP cannot sample the correct dielectric barrier in this situation.

Finally, consider the membrane with a narrow cylindrical pore (Figure 2b). In the following calculations the system geometry and the boundary concentrations are as before ($L_z = 66$ Å, $l = 24$ Å, $c_R = c_L = 0.1$ M), and the pore radius was taken to be $r_p = 4$ Å. It should be emphasized that this pore is represented only crudely by our low resolution grid: The grid spacing were taken to be 0.50 and 2.0 Å, respectively, for the PNP and the DLMC computations.

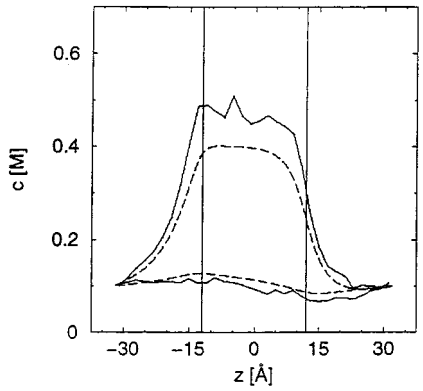

Figure 10. Concentration of positive ions along the channel axis for the system of Figure 2b. The pore's radius is $r_p = 4$ Å and its length is $l = 24$ Å. Equal salt concentrations $c = 0.1$ M were set on the L and R boundaries at $z = \pm 33$ Å. The dielectric constant is 80 everywhere. Full and dashed lines are respectively results of the DLMC and the PNP calculations. The lower pair of curves is for $\Delta\Phi = 50$ mV and the upper pair of curves corresponds to $\Delta\Phi = 300$ mV. The two vertical lines mark the positions of the channel openings.

There are several ways in which the confined nature of the ion passage through the channel may be misrepresented by the PNP approximation. First, the pore radius is not much bigger than the ion size (represented by the DLMC grid spacing); thus the effective pore cross section is overestimated in the PNP calculation that does not take into account short-range interactions that define the ion size. Similarly, the PNP theory also disregards the short-range part of the ion−ion interaction. Next, at the core of the PNP (and the PB) mean field approximation lies the interaction of any given ion with the average distribution of all other ions, *including the given ion itself*. This unphysical contribution to the ion energy is negligible in bulk systems containing many ions, but constitutes a substantial error in a narrow channel which sometimes contains no more than one ion (see below). Finally, the dielectric self-energy that appears as a substantial energy barrier to ion motion through a narrow channel is strongly underestimated by the PNP procedure.[20−24,58] This happens because in the PNP and PB theories ions are represented only by their average distribution, that is much broader than individual ion sizes.

In order to distinguish between these different effects we consider first a homogeneous dielectric channel with $\epsilon = 80$ everywhere. Figure 10 shows the average positive ion concentration as a function of position along the channel at two steady states with $\Delta\Phi = 50$ mV (lower lines) and $\Delta\Phi = 300$ mV (upper lines). The PNP (dashed lines) and DLMC (full lines) results differ from each other by $\sim$20%. When the system is driven by the higher potential there is an accumulation of ions near and inside the channel and the ion density in the channel becomes substantially higher. The PNP result is lower in this case than the DLMC result because it incorporates the unphysical self-interaction of the ions which essentially resists the "squeezing" of an ion through the channel. We note that the integrated average ion numbers for these cases are $\sim$0.31 (DLMC) and $\sim$0.29 (PNP), substantially less than 1.

The current−voltage characteristic of this channel is shown in Figure 11. The nominal channel cross section is $4\pi r_p^2 = 50.3$ Å^2, and this is the cross section relevant to the PNP calculation (dashed line). When the ion radius (1 Å) is taken into account, the effective channel cross section becomes 28.3 Å^2. (Because of our grid structure this is only a rough approximation to the effective cross-section on the grid.) In fact, two errors in the PNP model compensate each other in the numerical calcula-

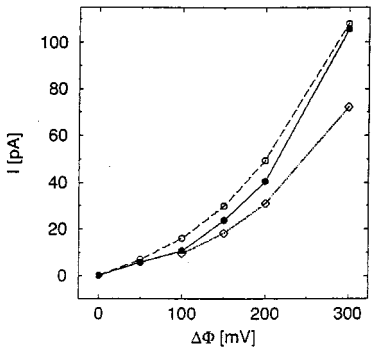

Figure 11. *I/V* characteristic for the same system as in Figure 10. Equal salt concentrations $c = 0.1$ M were set on the L and R boundaries at $z = \pm 33$ Å. Full line: result of the DLMC calculation. Dashed line: result of the corresponding PNP calculation. Dotted line: result of a PNP calculation with a pore radius $r_p = 3$ Å.

tion: First, the effective channel radius is overestimated by the lack of an intrinsic ion size, and, second, the unphysical self-repulsion inhibits its penetration into the channel. If we correct for the first error by taking a pore radius $r_p = 3$ Å in the PNP calculation (dotted line in Figure 11) the resulting current is lower than in the corresponding DLMC calculation because of the second error.

Of conceptual interest is the superlinear dependence of the current on the voltage seen (Figure 11) in both the PNP and the DLMC calculations. This behavior results from the fact that most of the voltage drop $\Delta\Phi$ occurs on the membrane (and across the channel), so for a constant ion concentration in the channel it leads to a linear dependence of I on $\Delta\Phi$. The fact that the ion density in the channel increases with $\Delta\Phi$, as seen in Figure 10, gives rise to the superlinear $I/\Delta\Phi$ characteristic seen in Figure 11.

It should be emphasized that, given the considerable conceptual differences between the PNP and DLMC methodologies, the results seen in Figures 10 and 11 show remarkable similarities. Far greater differences are encountered in the inhomogeneous dielectric case discussed below.

Next consider a channel with nonhomogeneous dielectric distribution, given by $\epsilon_s = 2$ in the membrane and $\epsilon_b = 80$ in the rest of the system, including the pore. As discussed above, and as already noted by several authors,[20−25,58] a high single-ion barrier in narrow channels, associated with the dielectric self-energy of the ion, is strongly underestimated in the PNP theory. For the geometry used before ($L_z = 66$ Å, $l = 24$ Å, and $r_p = 4$ Å) we find this barrier to be 4.3 k_BT ($T = 300$ K). Consequently, no appreciable current can go through this pore. In contrast, a PNP calculation yields a finite current due to the absence of the self-energy barrier. A more realistic configuration should take into account also permanent charges on the channel wall.[9−12,16] These charges lower the channel barrier for ions of the proper charge, enhancing the channel permeability and selectivity for this type of ions.

We have included such permanent charges in the model in the following way: the cylindrical pore ($r_p = 4$ Å) is surrounded by two cylindrical shells. An inner shell, $r_p < r \le r_1$, that carries a homogeneous charge distribution with a total charge Q, and an outer shell, $r_1 < r \le r_2$, with a homogeneous distribution of charge $-Q$. In the simulations described below we have used $r_1 = 5$ Å, $r_2 = 6$ Å, and $Q = -1.5$ e. Such a charge distribution by itself yields a potential well for the positive ion in mid-channel, of depth -1.6 k_BT, making the net potential barrier for this ion 2.7 k_BT.

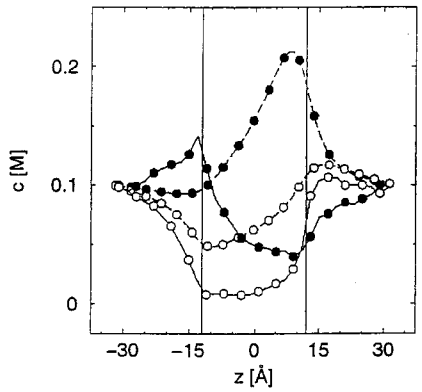

Figure 12. Concentration profiles along the pore axis, obtained for a pore radius $r_p = 4$ Å, with permanent charges distributed on the pore boundary surface as described in the text. The dielectric constant is 2 in the membrane, and 80 in the pore and the bathing solutions. The concentration boundaries are $c_L = c_R = 0.1$ M. The applied voltage boundary condition is $\Delta\Phi = 300$ mV. Full and dashed lines are respectively the DLMC and the PNP results, with filled circles describing the cations and open circles the anions. The two vertical lines mark the positions of the channel openings.

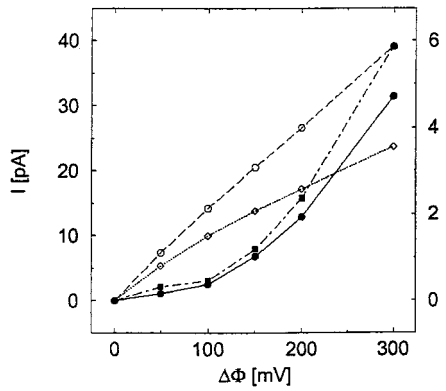

Figure 13. Current vs voltage results obtained from the DLMC simulation (full line with filled circles, associated with the right-side scale) and from the PNP approximation (dashed line with blank circles, left scale). The channel geometry, its dielectric structure, and the permanent charge distribution are as in Figure 12. These full and dashed lines are results obtained for a pore radius $r_p = 4$ Å. As discussed in the text, this pore radius should correspond to a smaller effective radius, $r_p = 3$ Å, in the PNP calculation (dotted line with blank squares, left scale). The dash−dotted line with filled squares (right scale) is the result of a DLMC calculation in which the Coulombic interaction between mobile ions where eliminated (i.e., each mobile ion moves independently of other mobile ions).

Figures 12 and 13 show, respectively, the ion concentration profiles and the current−voltage characteristic of this model system. The concentration profiles obtained from the PNP and the DLMC calculation are shown in Figure 12 to be markedly different from each other. In particular it is seen that in the PNP dynamics positive ions are attracted by the permanent charge distribution to the mid-pore region, but are repelled from this region in the DLMC dynamics which is still dominated by the dielectric barrier. These substantial differences in the description of the ionic distributions are expected to lead to similar differences in the current−voltage behavior of these models. Indeed, Figure 13 shows that the PNP calculation overestimates the total current by more than an order of magnitude, and is also unsuccessful in reproducing the super-linear behavior seen in the DLMC calculation.[59] On the other hand, it is seen that neglecting the interactions between mobile ions altogether (i.e., moving the ions under the effect of all but their mutual Coulombic interactions) provide a relatively good approximation

in this system, where the average ionic occupation in the channel is less than 1.

To summarize this section, we found that for a simple liquid junction with no geometrical restrictions on the ions' motion and no internal dielectric interfaces, the mean field (PNP) approximation and the particle lattice Monte Carlo dynamics give results that are in good agreement with each other. Since PNP is expected to be a reasonable approximation in this system (where correlation between ionic motions do not have a strong effect on dynamics) this could be regarded as a test of validity of our DLMC procedure. In the other situations considered the PNP theory shows various degrees of deviation from the more realistic description provided by the DLMC simulation of the particle-lattice model. These deviations are particularly severe in the description of ion transport through narrow dielectric channels, and casts doubts on previously published PNP results for ion transport through narrow membrane channels.[9−18] It should be emphasized that other factors, not taken into account in the present model, may lead to lower barriers in realistic channels (else ion transport through narrow channels such as gramicidin would not occur). This may result from a larger than assumed channel polarizability or from structural rearrangement in the channel in response to the passing ion.

9. Concluding Remarks

This paper has described a particle-level numerical approach to the study of ionic equilibrium and transport in systems that are (a) bounded by potential and concentration boundaries, and (b) may have internal dielectric inhomogeneities, including interfaces between solvents of different dielectric constants. The use of concentration and potential boundaries is standard in calculations based on coarse grained models such as the Poisson−Boltzmann and the Poisson−Nernst−Planck (drift-diffusion) theories. It is not straightforward in particle-level simulations, in particular those involving charged particles, and this paper has discussed some of the problems involved and has suggested ways to handle them.

An important feature of our simulated system is its identification as a small part of a larger embedding system. Focused attention on this small "inner" system is needed for numerical efficiency and is natural in the study of systems that are driven by local processes (i.e., ion transport through membrane channels). The resulting concentration and potential boundary conditions imposed on the inner system are restrictions only on the *average* values of these variables. We found that this has important consequences, in particular for the way the potential boundary is handled: a constant potential boundary condition responds to the individual motions of charged particles as a metal, while a constant average potential plane such as any plane cut in an equilibrium electrolyte solution does not. On the other hand, image effects associated with real internal dielectric boundaries have to be considered in full. Other, somewhat more subtle, issues include the need to account for the response of the imposed boundaries to the *average* charge distribution in the inner system and for the partial loss of solvation energy by an ion approaching these boundaries.

These and some other issues discussed in this work result from the artificial nature of the imposed interface between an external, continuum system characterized by average concentrations and electrostatic properties and an inner system described on the microscopic level. In the present work the simulation of the inner system is still restricted to a rather coarse grained level: the solvent is represented by a dielectric continuum and the ions are restricted to move on a grid. This level of description is sufficient for studying the limitations of mean field continuum theories (PB, PNP) of ionic systems. It leaves much to be desired in constructing realistic models for such systems. It obviously disregards the molecular nature of the solvent, but even as a continuum model it does not account for hydrodynamic flows and associated contributions to interionic interactions. On the other hand, we emphasize again that the methods developed here for handling concentration and potential boundary conditions will be useful also when more detailed microscopic descriptions of the inner system are used.

By comparing the results of our simulation procedure to these obtained from applying the PNP scheme on a system in which mean field approximation should provide a reasonable description, and by performing the other calibration tests described above, we have verified that our numerical scheme performs reasonably within the limitations of our numerical model. Further calculations that compare the performance of the PNP theory to the more rigorous DLMC dynamics have highlighted some severe shortcomings of the mean-field approach to ion transport in inhomogeneous dielectric media. In agreement with recent Brownian dynamics simulations,[20−25] we have to conclude that earlier PNP work on ion transport through biological channels[9−18] have to be reassessed with care.

Finally, the observation that self-energy of the mobile ion in the inhomogeneous dielectric environment is a major factor in the difference between results obtained from the DLMC and the PNP methodologies offers a way to substantially improve the performance of the latter mean field approximation. This is based on the fact that the dielectric self-energy, being a single ion property, is included as an additive term in the energy used in the PB and PNP calculations; see dotted line in Figure 8a. Furthermore, including, on the mean field level, effects of finite ion sizes can also increase the accuracy and applicability of this approximation. These issues will be discussed in detail elsewhere. At the same time it should be emphasized again that the calculations presented here and in refs 23, predict solvation barriers that are unrealistically high. For a narrow channel like Gramicidin A (radius of about 2 Å), the solvation barrier is 20−40 k_BT if the dielectric constant of the aqueous region is 80 everywhere and that of the protein-membrane region is 2.[58] This effect must somehow be suppressed, because if it were not, no ions could permeate through the GA channel under any physiologically relevant conditions, whereas in reality cations permeate easily through GA under such conditions. This suggests that other factors, not taken into account by the present electrostatic models, must play a role in lowering the activation barrier for ion transmission through narrow membrane channels. Such additional mechanisms may include the following: (1) configurational fluctuations of the protein channel, (2) a higher dielectric constant in the protein, due to a larger polarizability than that of the lipid bilayer membrane,[60] and (3) strong attractive chemical interactions between the permeating ion and particular function groups in amino acids lining the walls of the pore. Further investigation of these features would be of considerable interest.

Appendix A. The PNP Equations

Here we briefly outline the structure of the steady-state Poisson−Nernest−Planck (PNP) equations. These equations combine the Poisson eq 1 for the electrostatic potential associated with a given distribution of fixed charges ρ_f and *average* charge distribution of mobile ions

$$-\nabla\cdot[\epsilon(\mathbf{r})\nabla\phi(\mathbf{r})] = 4\pi[\rho_f(\mathbf{r}) + \sum_{i=1}^{N} z_i e c_i(\mathbf{r})] \quad \text{(A1)}$$

and the steady-state drift-diffusion equations for the fluxes of the mobile ions

$$0 = \nabla\cdot\mathbf{j}_i = \nabla\cdot[-D_i(\nabla c_i(\mathbf{r}) + \beta c_i(\mathbf{r})\nabla V_i(\mathbf{r}))]; \quad i = 1, ..., N \quad \text{(A2)}$$

where $V_i(\mathbf{r}) = z_i e\phi(\mathbf{r})$ accounts for the interionic interaction on the mean field level. A reasonable modification takes

$$V_i(\mathbf{r}) = U(\mathbf{r}) + z_i e\phi(\mathbf{r}) \quad \text{(A3)}$$

where U is the single particle potential (local solvation energy) associated with the inhomogeneous solvent. In these equations c_i, j_i, z_i, and D_i are repectively the concentrations, fluxes, valences, and diffusion constants of the ion species ($i = 1, ..., N$). e is the magnitude of the electron charge and $\beta = (k_B T)^{-1}$. The one-particle potential U is sometimes taken into account only implicitly by using reflecting boundary conditions that prevent ion entrance into nondielectric environments. An implementation of Eqs (A1,2) to ion diffusion through membrane channels was described in our earlier work.[16] Under equilibrium conditions, where all j_i vanish and $c_i \sim \exp(-\beta z_i e\phi)$, these equations reduce to the Poisson−Boltzmann equations.

Appendix B. Numerical Solution of the Poisson Equation on a Lattice

Here we briefly describe the procedure used for solving the Poisson equation on a cubic grid. This is a standard method[61] and is included here in order to define our notation. The following outline is written using a one-dimensional language but is easily generalized to any number of dimensions. The real space coordinates (up to a translation) of the lattice sites are

$$x_j = jh, \quad j = 1, 2, ..., n \quad \text{(A4)}$$

with $h > 0$. A lattice cell extends from $(j - 1/2))$ to $(j + 1/2)h$. The volume of one lattice cell is denoted by V_h. For periodic boundary conditions, the formal identities $x_0 \equiv x_n$ and $x_{n+1} \equiv x_i$ are employed. For a direction in which the system is bounded, x_0 and x_{n+1} are identified with the boundaries L and R introduced in section 3. In both cases, the cells associated with the sites labeled by $j = 1, ..., n$ cover the interior system. The value $f(x_j)$, which a function f assumes on a lattice site j, is denoted by f_j.

Next, the Poisson eq 1 is discretized on this grid. The finite volume method is suitable for discretization of differential equation with discontinuous parameters.[62] In this method, the differential equation is integrated over a lattice cell and interfacial continuity conditions are utilized across the surface of lattice cells. For our problem, this method corresponds to allowing discontinuities in the dielectric profile at the surfaces of lattice cells, while assuming continuous variation of $\epsilon(\vec{r})$ over the interior of the cells. When applied to the differential equation

$$\frac{d}{dx}\left[a(x)\frac{du(x)}{dx}\right] = b(x) \quad \text{(A5)}$$

this method, with the requirement of continuity of $u(x)$ and $a(x)$ $du(x)/dx$ yields

$$\frac{1}{h^2}\frac{2a_j a_{j+1}}{a_j + a_{j+1}}(u_{j+1} - u_j) - \frac{1}{h^2}\frac{2a_{j+1}a_j}{a_{j-1} + a_j}(u_j - u_{j-1}) = b_f \quad \text{(A6)}$$

This can be generalized to the discretization of eq 1. Moving fixed boundary terms to the right this finally yields

$$\sum_j L_{ij}\phi_j = b_i^{(\rho)} + b_i^{(D)} \quad \text{(A7)}$$

where the index j now denotes a lexical index identifying a site on the 3-dimensional lattice, L_{ij} is the 3-dimensional generalization of the matrix defined by eq A6 (a_j becomes the dielectric constant on site j), $b_i^{(\rho)} = -4\pi\rho_{free}(\vec{r})$ and $b_i^{(D)}$ are effective source terms associated with the Dirichlet (potential) boundary condition. In addition to eq A7 we sometimes solve identical reference equations for systems in which ϵ is uniformly 1 (the corresponding matrix is then denoted $L_{ij}^{(0)}$) or some other uniform value ϵ_B (with the corresponding matrix L_{ij}^{B}).

Appendix C. Numerical Efficiency Issues

The main numerical difficulty encountered in simulating inhomogeneous electrolyte systems is the calculation of the electrostatic response associated with the dielectric inhomogeneity, i.e., ϕ^{diel} of section 6c. Repeated numerical solution of the Poisson equation during each Monte Carlo cycle is not practical. Precalculating and storing, e.g., $\phi_{j\leftarrow k}^{diel}$ for all lattice sites k and restoring it during the Monte Carlo simulation also stretches the limits of computational and memory resources. We note that in related studies[20−25] cylindrical symmetry was used to reduce the storage memory problem. Here we describe another method that does not rely on geometrical symmetry (the latter can be used in addition). We assume that the interior system may be divided into two regions I and II, as in Figure 2b; the dynamics is controlled by ion motion in region I and interactions involving ions in this region are captured exactly. The dynamics is less sensitive to ionic motion in region II, and their interactions may be considered in some approximation (that becomes better when region I is larger). For the particular system depicted in Figure 2 the following procedure can be used:

The functions $\phi_{j\leftarrow k}^{diel}$, eq 21, are precalculated and stored for all lattice sites k in region I (Figure 2). This involves storage of $(N_I + N_{II})N_I$ numbers, where N_I and N_{II} are the number of grid points in region I and II of the interior system. This number is substantially smaller than the number $(N_I + N_{II})^2$ that is the order of magnitude required to store all relevant electrostatic information.

The pair interaction between two ions is computed as follows:

If either of the two ions is located within region I, then the precalculated functions $\phi_{j\leftarrow k}^{diel}$ are available, and the interaction potential is given by eq 22 multiplied by $q_j q_k$ Because of the symmetry property (23), the same function can be used for computing the "dielectric polarization interaction" of an ion located inside region I with another ion at an arbitrary location and vice versa.

If both ions are located in region II, their interaction is calculated as if there was no pore. The system without a pore (bath|slab|bath) is highly symmetric, and only a small set of functions $\phi_{j\leftarrow k}^{diel}$ has to be precalculated and stored for such a system. This approximation becomes better when the size of region I is larger; the ensuing error for the system of Figure 2 can be made of the order of a few percent of the thermal energy $k_B T$ at room temperature.

Acknowledgment. This research was supported in part by the Israel Science Foundation (AN) and by the National Institute of Health (Grant GM61082-01) and the Petroleum Research Fund (Grant 34754-AC6)(RDC). P.G. and A.N. thank Boaz Nadler, Tamara Naeh, and Zeev Schuss for discussions on numerical approaches to inhomogeneous electrolyte systems and to embedding issues. M.K. and R.D.C. thank Alfredo Cardenas for extensive discussions on the topic of ion permeation.

References and Notes

(1) Schmickler, W. *Interfacial Electrochemistry*; Oxford University Press: New York, 1996.

(2) Bockris, J. O'M.; Khan, S. U. M. *Surface Electrochemistry. A molecular level approach*; Plenum Press: New York, 1993.

(3) Gray, F. M. *Solid Polymer Electrolytes. Fundamentals and technological applications*; VCH: Weinheim, Germany, 1991.

(4) Hille, B. *Ionic Channels of Excitable Membranes*, 2nd ed.; Sinauer Associates, Inc.: Sunderland, MA, 1992.

(5) Levitt, D. G. *J. Gen. Physiol*. **1999**, *113*, 789.

(6) Nicholls, A.; Sharp, K. A.; Honig, B. DelPhi V3.0; Columbia University, New York, 1990.

(7) Honig, B.; Sharp, K.; Yang, A. S. *J. Phys. Chem*. **1993**, *97*, 1101.

(8) Honig, B.; Nicholls, A. *Science* **1995**, *268*, 1144.

(9) Eisenberg, R. S. *J. Membr. Biol*. **1996**, *150*, 1.

(10) Eisenberg, R. S. *Acc. Chem. Res*. **1998**, *31*, 117.

(11) Eisenberg, R. S. *J. Membr. Biol*. **1999**, *171*, 1.

(12) Nonner, W.; Chen, D. P.; Eisenberg, R. S. *J. Gen. Physiol*. **1999**, *113*, 773.

(13) Syganow, A.; von Kitzing, E. *J. Phys. Chem*. **1995**, *99*, 12030.

(14) Syganow, A.; von Kitzing, E. *Biophys. J*. **1999**, *76*, 768.

(15) Syganow, A.; von Kitzing, E. *Eur. Biophys. J*. **1999**, *28*, 393.

(16) Kurnikova, M. G.; Coalson, R. D.; Graf, P.; Nitzan, A. *Biophys. J*. **1999**, *76*, 642.

(17) Cárdenas, A. E.; Coalson R. D.; Kurnikova, M. G. *Biophys. J*. **2000**, *79*, 80.

(18) Hollerbach, U.; Chen, D. P.; Busath, D. D.; Eisenberg, B. *Langmuir* **2000**, *16*, 5509.

(19) See, e.g., Caillol, J. M. *J. Chem. Phys*. **1999**, *111*, 6528, and references therein.

(20) Chung, S.-Ho; Hoyles, M.; Allen, T.; Kuyucak, S. *Biophys. J*. **1998**, *75*, 793.

(21) Hoyles, M.; Kuyucak, S.; Chung, S.-Ho *Phys. Rev. E* **1998**, *58*, 3654.

(22) Corry, B.; Kuyucak, S.; Chung, S.-Ho *J. Gen. Physiol*. **1999**, *114*, 597.

(23) Chung, S. H.; Allen, T. W.; Hoyles, M.; Kuyucak, S. *Biophys. J*. **1999**, *77*, 2517.

(24) Allen, T. W.; Hoyles, M.; Kuyucak, S.; Chung, S. H. *Chem. Phys. Lett*. **1999**, *313*, 358.

(25) Three relevant papers have appeared after our paper was submitted. (a) Moy, G.; Corry, B.; Kuyucak, S.; Chung, S.-Ho *Biophys. J*. **2000**, *78*, 2349−2363, 2364−2381, describes Brownian dynamics simulations of ion transport through a pore with comparison to mean field (PB and PNP) calculations. Our methodology is different from the approach taken in these papers. Nevertheless our results are consistent with the observations made in these works. (b) Im, W.; Seefeld, S.; Roux, B. *Biophys. J*. **2000**, *79*, 788, describes a Brownian dynamics simulation of ion motion in a Porin channel. In this paper dielectric effects on self-energy and interparticle interactions of mobile ions are disregarded.

(26) Elber, R.; Chen, D. P.; Rojewska, D.; Eisenberg, R. *Biophys. J*. **1995**, *68*, 906.

(27) Woolf, T. B. and Roux, B. *Biophys. J*. **1997**, *72*, 1930.

(28) Tieleman, D. P.; Berendsen, H. J. C. *Biophys. J*. **1998**, *74*, 2786.

(29) Knödler, D.; Pendzig, P.; Dieterich, W. **1994**, *70*, 356.

(30) Knödler, D.; Dieterich, W.; Lonsky, C.; Nitzan, A. *J. Chem. Phys*. **1995**, *102*, 465.

(31) Pendzig, P.; Dieterich, W.; Nitzan, A. *J. Noncryst. Solids*. **1998**, *235*, 748.

(32) For an impressive demonstration of such a program in the study of fracture dynamics in silicon see: Abraham, F. F.; Broughton, J. Q.; Bernstein, N.; Kaxiras, E. *Comput. Phys*. **1998**, *12*, 538.

(33) A description of an *equilibrium* ionic channel in which the system is separated into an inner and an outer subsystems was recently presented by: Roux, B. *Biophys. J*. **1999**, *77*, 139.

(34) See, e.g.: Barcilon, V.; Chen, D.; Eisenberg, R. S.; Ratner, M. A. *J. Chem. Phys*. **1993**, *98*, 1193.

(35) Böttcher, C. J. F. *Theory of Electric Polarization. Dielectrics in Static Fields*, 2nd ed.; Elsevier: New York, 1973.

(36) Shaw, P. B. *Phys. Rev. A* **1985**, *32*, 2476.

(37) Newton, M. D.; Friedman, H. L. *J. Chem. Phys*. **1988**, *88*, 4460.

(38) In the application of these periodic boundary conditions in the present work the corresponding interion interactions were computed with the minimum image approximation.

(39) For example, composite grids could be used: one grid for the calculation of the electrostatic potential and a different, finer grid to represent ion configuration and ionic motion where the ion occupies more than a single grid cell. For the use of composite grids in electrostatic calculations see: Beck, T. L. *J. Comput. Chem*. **1999**, *20*, 1731−1739.

(40) Binder, K.; Heermann, D. W. *Monte Carlo simulation in statistical physics*; Springer-Verlag: New York, 1988.

(41) See, e.g.: Binder, K. Monte Carlo Investigations of Phase Transitions and Critical Phenomena. *Phase Transitions and Critical Phenomena*; Academic Press: New York, 1976; Vol. 5b, Chapter 1, pp 1−105.

(42) In practical applications a may be fitted to the experimental solvation energy using the Born expression for the solvation energy $W = (q^2/(2a))(1/\epsilon - 1)$.

(43) Using Coulomb potentials with a cutoff is a potential source of error. Alternatively, using Ewald summation in inhomogeneous restricted geometry systems (in our case a 2-dimensional Ewald summation is required) is computationally very demanding. Moreover, the inhomogeneous net charge distribution of mobile ions in our system would lead to unphysical interactions between periodic extensions of the system in the Ewald method. There are indications that the errors introduced by using Coulomb interactions with cutoff are not very large for many applications, see, e.g.: Schweighofer, K.; Benjamin, I. *J. Chem. Phys*. **2000**, *112*, 1474−1482 and references therein. Controlling these errors is important in situations where system properties are dominated by the balance between opposing interactions, e.g., Coulombic repulsion vs dielectric attraction in solvated ions of the same charge sign (Bader, J. S.; Chandler, D. *J. Phys. Chem*. **1992**, *96*, 6423).

(44) In continuous space the potential of eq 12 corresponds to a charge distribution where the ion charge is uniformly spread over the surface of a sphere with radius a, whose center is the ion position, and an additional charge of exactly the opposite magnitude uniformly spread over the surface of the cutoff sphere $r = r_c$.

(45) The structure of $L^{(0)}$ reflects in the usual way the periodic boundary condition in the x- and y-direction and the finite system size in the z-direction.

(46) Charge redistribution based on more heuristic procedures is used in other grid based numerical approaches to electrostatic problems, e.g., the Delphi code.[6]

(47) The unphysical image of polarization charges, induced by individual ions on the internal dielectric interfaces, on the imposed boundaries is not eliminated by this procedure. If, however, the imposed boundaries are far from the dielectric interfaces the resulting unphysical contribution to the total energy is small.

(48) The analytical results used in Figures 3 and 4 are obtained from classical electrostatics (Jackson, J. D. *Classical electrodynamics*, 2nd ed.; Wiley: New York, 1975): An ion of charge q is placed in a semi-infinite medium 1 of dielectric constant ϵ_1, at position (0, 0, −d), and a planar interface $z = 0$ separates medium 1 from another semi-infinite medium 2 of dielectric constant ϵ_2. The potential in medium 1 is the combination of potentials from the original charge and the image charge $q' = (\epsilon_1 - \epsilon_2)/(\epsilon_1 + \epsilon_2)q'$ located on the normal from the real charge to the interface, a distance $2d$ from the real charge inside medium 2. The self-energy plotted in Figure 3 is the sum of charging energies, $q^2/(2\epsilon_1 a) + qq'/(4\epsilon_1 d)$, of the ion (taken to have a radius a), one contribution due to the dielectric solvent, the other due to the image interaction. The potential plotted in Figure 4 is $\Phi(\mathbf{r}) = q'/(\epsilon_1 R_2)$ for $z < 0$ and $\Phi(\mathbf{r}) = q''/(\epsilon_2 R_1) - q/(\epsilon_1 R_1)$; $q'' = (2\epsilon_2)/(\epsilon_1 - \epsilon_2)$ for $z > 0$, where $R_1 = |\mathbf{r} - (0, 0, -d)|$, and $R_2 = |\mathbf{r} - (0, 0, d)|$ are the distances between point $\mathbf{r}$ and the charges q and q', respectively. (Note that we compute here only the *polarization contribution* to the potential Φ. These expressions, which diverge on the interface, become valid far enough (from distances of order a, or our grid spacing) from the interface. See: Khurkats, Y. I.; Ullstrup, J. *J. Electroanal. Chem*. **1991**, *308*, 17−26 for a discussion of this point.

(49) As in section 6b, a part that is not eliminated comes from the image of the polarization charges induced at the internal dielectric boundaries; however, this contribution can be made small (see footnote 47).

(50) $\epsilon_B = 80$ is used in all calculations reported here, because in anticipated applications ions reside in a water environment.

(51) An alternative procedure would be to calculate the contribution of the outer medium to the solvation energy of an ion near the boundary using, e.g., a Poisson−Boltzmann description of the outer medium (see, e.g.: Sadus, R. J. *Molecular Simulations of Fluids*; Elsevier: Amsterdam, 1999). This would, however, raise the issue of validity of the PB approximation for computing solvation energies near a system's boundary.

(52) See for example: McQuarry, D. A. *Statistical Mechanics*: Harper & Row: New York, 1976.

(53) Mafé, S.; Pellicer, J.; Aguilella, V. M. *J. Phys. Chem*. **1986**, *90*, 6045.

(54) Aguilella, V. M.; Mafé, S.; Pellicer, J. *Electrochim. Acta* **1987**, *32*, 483.

(55) Riveros, O. J.; Croxton, T. L.; Armstrong, W. McD. *J. Theor. Biol.* **1989**, *140*, 221.

(56) In fact, the correspondence between the two approaches is not complete because the PNP theory disregards the retarding effect of the ionic solvation atmosphere on an ion's motion. This retardation affects the conductivity of a dilute homogeneous electrolyte solution by a few percent.

(57) In the corresponding PNP and PB calculation we used $c_L = c_R = 0.096$ M that correspond to the bulk concentration obtained in the equilibrium DLMC simulation. See Figure 5 and ensuing discussion.

(58) Dieckmann, G. R.; Lear, J. D.; Zhong, Q.; Klein, M. L.; DeGrado, W. F.; Sharp, K. A. *Biophys. J.* **1999**, *76*, 618.

(59) In realistic biological channels, which may contain internal structural barriers, blocking of ionic motion as a result of ions being trapped for a relatively long time inside the channel may actually lead to a sublinear $I/\Delta\Phi$ characteristic. See, e.g.: Andersen, O. S. *Biophys. J.* **1983**, *41*, 135.

(60) Sham, Y. Y.; Muegge, I.; Warshel, A. *Biophys. J.* **1998**, *74*, 1744−1753. (b) Muegge, I.; Schweins, T.; Warshel, A. *Proteins: Struct. Funct. Genet.* **1998**, *30*, 407−423. (c) Simonson, T.; Brooks, C. L. *J. Am. Chem. Soc.* **1996**, *118*, 8452−8458.

(61) See, e.g.: Press: W. H.; Teukolsky, S. A.; Vetterling, W. T.; Flannery, B. P. P. *Numerical Recipes in FORTRAN: The Art of Scientific Computing*, 2nd ed.; Cambridge University Press: London, 1992.

(62) Wesseling, P. *An Introduction to Multigrid Methods*; John Wiley & Sons Ltd.: Chichester, UK, 1992.